Renewable Energy 165 (2021) 369–380

Contents lists available at ScienceDirect

Renewable Energy

journal homepage: www.elsevier.com/locate/renene

Quantifying the technical geothermal potential from shallow borehole heat exchangers at regional scale

Alina Walch [a, *], Nahid Mohajeri [b], Agust Gudmundsson [c], Jean-Louis Scartezzini [a]

[a] Solar Energy and Building Physics Laboratory, Ecole Polytechnique Federale de Lausanne, Switzerland
[b] UCL Institute for Environmental Design and Engineering, University College London, London, United Kingdom
[c] Department of Earth Sciences, Royal Holloway University of London, Egham, United Kingdom

ARTICLE INFO

Article history:
Received 3 July 2020
Received in revised form
29 September 2020
Accepted 6 November 2020
Available online 10 November 2020

Keywords:
Shallow geothermal energy
Borehole heat exchangers
Potential estimation
Numerical modelling
Geographic information systems

ABSTRACT

The extraction of shallow geothermal energy using borehole heat exchangers (BHEs) is a promising approach for decarbonisation of the heating sector. However, a dense deployment of BHEs may lead to thermal interference between neighboring boreholes and thereby to over-exploitation of the heat capacity of the ground. Here we propose a novel method to estimate the technical potential of BHEs which takes into account potential thermal interference as well as the available area for BHE installations. The method combines simulation of the long-term heat extraction through BHEs for a range of borehole spacings and depths and includes an optimisation step to maximise the heat extraction. Application of the method to a case study in western Switzerland, from an available area of 284 km^2, yields an annual technical potential of 4.65 TWh and a maximum energy density of 15.5 kWh/m^2. The results also suggest that, for a minimum borehole spacing of 5 m and a maximum borehole depth of 200 m, the cumulative installed borehole depth should not exceed 2 km/ha. The estimated technical potential can be used by urban planners for the techno-economic analysis of BHE systems and by policy makers to develop strategies that encourage the use of shallow geothermal energy.

1. Introduction

The heating and cooling of buildings represents one third of Switzerland's total energy demand. Roughly 75% of this energy is supplied through fossil fuels, which account for 27% of the national CO_2 emissions [1]. Replacing fossil fuels with renewable heat sources can therefore reduce carbon emissions significantly. One abundantly available source of renewable heat is low-temperature shallow geothermal energy, which is defined as heat extracted from the ground at a depth of <400 m that is used directly for heating and cooling applications [2]. Ground-source heat pumps (GSHPs) are one technology to extract this energy by combining borehole heat exchangers (BHEs) with a heat pump (HP) [3]. As the ground temperature at the depth of the BHEs is nearly constant throughout the year, these systems have a high coefficient of performance (COP) and may even be used in a bi-directional way for both heating in winter and cooling in summer [4].

Despite its promising performance, a dense installation of GSHPs may lead to an over-exploitation of the heat capacity of the ground, caused by the thermal interference between neighboring boreholes [5]. This thermal interference and the available area for the installation of BHEs limit the technical potential of GSHPs, which is defined as the maximum annual heat energy that may be extracted using GSHP systems [6]. To quantify the technical potential of GSHPs, it is therefore crucial to account for the potential over-exploitation of the heat capacity of the ground [7]. The estimation should further be independent of the heat demand, for example when assessing the possible use of shallow geothermal energy in district heating networks. To support urban planners and policy makers, the technical potential needs to be estimated at the scale of entire regions, in order to highlight regional differences and particularly suitable areas for BHE installation. Currently, no regional-scale method exists to quantify a demand-independent technical potential for GSHPs that accounts for both the potential thermal interference and the available area for the installation of BHEs [8].

Instead of estimating the technical potential, most existing regional-scale geothermal studies estimate the theoretical potential, defined as the physically available energy in a given ground

* Corresponding author.
E-mail address: alina.walch@epfl.ch (A. Walch).

https://doi.org/10.1016/j.renene.2020.11.019

volume [8]. Studies of the theoretical potential include the estimation of ground temperature [9], heat capacity [10] and thermal conductivity [11]. These parameters are mapped from the thermal properties of the rock types [12,13], from 3D models of the subsurface [14], using kriging [15] and/or applying Machine Learning algorithms [16]. Hydro-geological data may further be used to estimate the rate of groundwater flow (Darcy velocity), which can have an important impact on the theoretical potential [17,18]. Several regional-scale studies quantify the extractable heat from a single borehole, which is estimated using engineering norms [19], simulation tools [20], or analytical models [21,22]. While these studies highlight areas with a high potential, they neglect the impact of the built environment and possible interaction and interference between boreholes, which are the focus of this work.

The estimation of the technical potential, accounting for the effects of a dense deployment of BHEs, requires the identification of a suitable number of boreholes per unit area in addition to the energy yield of individual BHEs. So far, this aspect has only been considered at the scale of neighborhoods [6], districts [23] or cities [24]. In these studies, a large number of BHEs with a spacing of $6-7.5$ m have been simulated, using a combination of Geographic Information Systems (GIS) and analytical or empirical models. The thermal interference between the BHEs at the neighborhood scale is only taken into account by Miglani et al. [6]. Neglecting thermal interference is only appropriate if the BHEs spacing exceeds half the borehole depth [25]. Such distances have been used by [26,27]. While the proposed borehole spacing of $6-7.5$ m yields an optimistic estimate of the technical potential, a spacing of half the borehole depth leads to a conservative estimate. The impact of borehole spacing on the performance of GSHPs has been studied conceptually for a fixed set of BHE configurations [28,29] and for BHEs in an infinite regular grid [5,30]. The performance drop as a result of closely spaced BHEs has been simulated so as to optimise the arrangement of BHEs in a single field [31] and to compute the maximum acceptable power in the proximity of existing installations [32]. To the best of our knowledge, these concepts are yet to be applied to study areas beyond neighborhood scale.

In this study, we quantify the effects of thermal interference between boreholes on the technical potential of GSHPs at the regional scale. In particular, we assess the impact of the built environment, the spacing between boreholes and the borehole depth on the maximum extractable heat. For the first time, we simulate the thermal interference between BHEs for a range of borehole spacings ($5-100$ m) and depths ($50-200$ m) at regional scale. Based on the simulation results, we propose an optimal arrangement of boreholes that maximises the technical potential while assuring a reasonable heat extraction power. In the paper, we consider only vertical closed-loop GSHP systems because these are the most commonly used systems in Switzerland [33]. The present study focuses on heat extraction from the ground and does not consider possible re-charging of the ground with heat from excess solar thermal generators or space cooling during hot summer days. The technical potential estimated here should therefore be regarded as conservative. The proposed method is applied to two cantons (Geneva and Vaud) in western Switzerland with over 80,000 parcels, each representing one property unit. The results yield a first regional-scale estimate of the technical potential of GSHPs in the two cantons.

2. Methods and data

The proposed method to quantify the technical potential of GSHPs combines (i) GIS processing for the virtual installation of BHEs for various density scenarios, where each scenario is defined by a different spacing between adjacent BHEs, (ii) analytical modelling of the borehole thermal response and its effect on the heat extraction power and the energy potential of the BHEs within each parcel and (iii) an optimisation step to maximise the energy potential of each parcel while assuring a minimum heat extraction power (see Fig. 1). The technical potential represents the annual heat energy that can be extracted from all the BHEs, such that their long-term operation is assured. We use a planning horizon (t_{dim}) of 50 years as suggested by the geothermal norm of the Swiss society of engineers and architects (SIA) [34]. The SIA norm defines the requirements for the dimensioning of shallow GSHPs in Switzerland and sets the technical framework for our work.

2.1. GIS processing for identifying potential BHE arrangements

To estimate the number of BHEs and their location for different scenarios of installation density, we propose a two-stage GIS-based approach. In the first stage, we estimate the available area for the installation of BHEs within each parcel. In the second stage, we virtually install BHEs on this available area for each scenarios of installation density, yielding a set of borehole fields.

To quantify the available area for the installation of BHEs, we combine parcel boundary data with building footprints and other artificial and natural landscape features, obtained from a Topographic Landscape Model (TLM). All parcels containing at least one building within their boundaries are considered. Parcels without any building inside are neglected, as these parcels neither create a demand for heating nor do they provide any infrastructure to install a GSHP system. From the selected parcels, we remove any built-up areas, such as building footprints, roads, railways, traffic-related areas (e.g. parkings, airports) and leisure zones (e.g. sport facilities). A buffer of 3 m is removed around all parcels and buildings to assure the minimum distance from a BHE to any building or parcel boundary as specified by the SIA [34]. We also exclude natural and artificial surface water bodies, natural habitat such as forests and wetlands, and protected areas such as national parks. Fig. 2 shows an example of the excluded objects and the available area within each parcel (blue shading).

To virtually install BHEs on the available area for all density scenarios, we arrange them on a rectangular grid with varying borehole spacing B. The lower bound for the spacing (B_{min}) is given by the SIA norm as 5 m [34]. The upper bound B_{max} equals half of the maximum borehole depth H_{max}, as interactions between BHEs with a spacing exceeding half the borehole depth are small [25]. As thermal interference decreases logarithmically with borehole spacing [35], we choose the density scenarios to resemble such a pattern (see Table 1). The virtual installation of BHEs for two example scenarios ($B = 5$ m, $B = 25$ m) is shown in the bottom left part of Fig. 2. The available area within each parcel yields the separate borehole fields.

2.2. Analytical model for quantifying the heat extraction potential

The analytical model introduced by Eskilson [35] is used to simulate the borehole thermal response and to derive the heat extraction potential of each field of BHEs. As the thermal response describes the thermal resistance of a BHE as a function of distance and time, it allows to quantify possible interaction effects between nearby boreholes. The model represents each BHE as a Finite Line Source (FLS), from which energy is extracted by conductive heat transfer. Additional heat transfer from groundwater flow is neglected in the model, which may result in some differences between the estimated and the real technical potential. The simulation of the heat extraction potential requires three types of inputs, namely (i) ground data, (ii) technical parameters and (iii) design

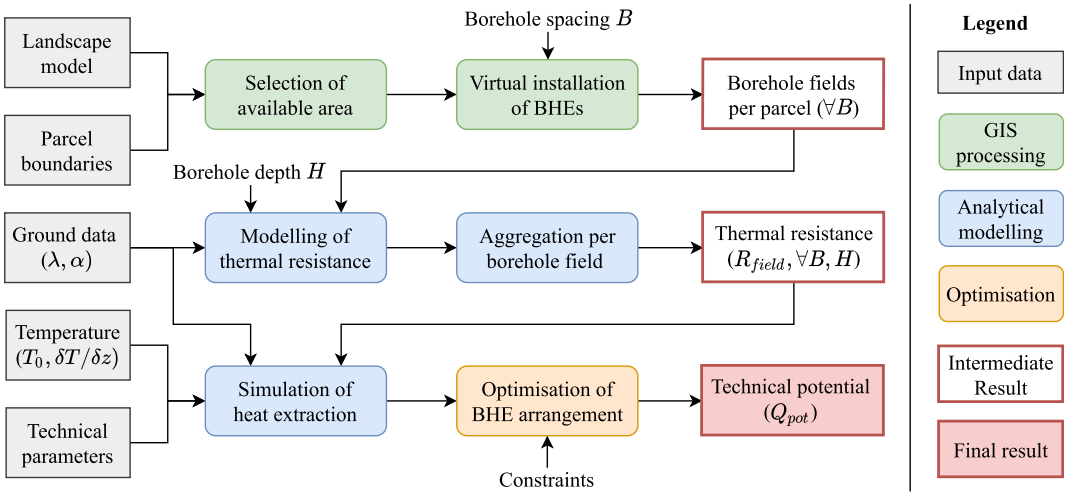

Fig. 1. Workflow for modelling the technical potential of GSHPs.

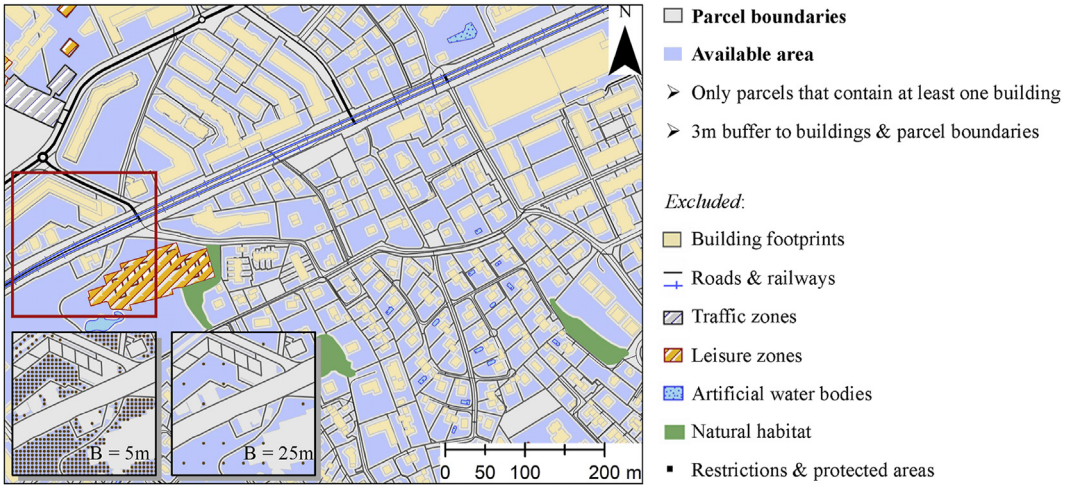

Fig. 2. Sample map showing the parcel boundaries, the available area and the excluded areas according to the Topographic Landscape Model. At the bottom left, the virtual installation of BHEs is shown for two example scenarios (BHE distances B = 5 m, B = 25m) for the area inside the red box. (For interpretation of the references to colour in this figure legend, the reader is referred to the Web version of this article.)

variables. The ground data are the thermal conductivity (λ), the thermal diffusivity (α), and the undisturbed ground temperature (T_g), which is computed at any depth z from the annual mean surface temperature (T_0) and the temperature gradient ($\delta T/\delta z$) as [34]:

$$T_g(z) = T_0 + z \times \frac{\delta T}{\delta z} - 1^\circ C \quad (1)$$

where the 1° C is a tolerance that is subtracted to account for uncertainties in the estimation of T_0. The λ and α have been derived from 3D models of the subsurface for various depths [36,37], T_0 has been estimated from measurement data [16] and $\delta T/\delta z$ is constant (see Table 1).

The technical parameters include the borehole thermal resistance (R_b), the borehole radius (r_b) and the annual operating time of the BHEs (t_{op}), defined as the typical number of full-load hours of a heat pump at a given altitude [34]. The design variables are the free parameters in the dimensioning of BHEs and must be selected in order to maximise the technical potential. These are the borehole depth (H), the borehole spacing (B) and the heat extraction rate (q_{max}). A complete list of all parameters, their units, values/ranges (for spatially varying data) and sources is provided in Table 1.

To compute the annual extractable energy for a BHE field (Q_{field}), Eq. (2) is used [25]:

$$Q_{field} = q_{max} \times t_{op} \times H \times N_B \quad (2)$$

where N_B is the number of BHEs in a field with spacing B. All N_B BHEs within one field are assumed to have an equal H and q_{max}. As our definition of the potential is independent of the heat demand, we aim to find q_{max} for a given H and N_B. To obtain q_{max}, we follow the standard design procedure for geothermal installations [25,38,39]. According to this procedure, GSHP systems for heating are designed such that the mean temperature of the heat carrier fluid (T_{mf}) inside the borehole remains above a minimum value $T_{mf,min}$, given as −1.5° C in the norm [34], throughout t_{dim}. Rearranging the expression for $T_{mf,min}$, we compute q_{max} for each BHE field and each given B and H as shown in Eq. (3) (cf [25]):

Table 1
Description of variables and parameters used in this work. The ground data and H_{max} are specific for the case study area and will be detailed in Section 3. Values in brackets represent averages across the study region.

Type	Symbol	Unit	Description	Value/range	Source
Ground data	λ	W/mK	Thermal conductivity	1.6 – 3.0 (2.4)	ASIT-VD [36], SITG [37]
	α	$\mu m^2/s$	Thermal diffusivity	0.6 – 1.4 (1.1)	ASIT-VD [36], SITG [37]
	T_0	°C	Surface temperature	8 – 11 (10.4)	Assouline et al [16].
	$\delta T/\delta z$	K/m	Temperature gradient	0.03	SIA norm [34]
Technical parameters	$T_{mf,min}$	°C	Minimum fluid temperature	− 1.5	SIA norm [34]
	t_{dim}	a	Planning horizon	50	SIA norm [34]
	t_{op}	h	Annual operation time	1800 – 2000 (1830)	SIA norm [34]
	r_b	m	Borehole radius	0.065	Perego et al. [13], Miglani et al. [6]
	R_b	mK/W	Effective borehole resistance	0.15	Rivera et al [5].
	$w_{hdd,max}$	−	Maximum HDD weight	0.16 – 0.20 (0.19)	Eq. (6), Appendix B
Design variables	q_{max}	W/m	Maximum heat extraction rate	*Target variable*	
	H	m	Borehole depth	{50, 100, 150, 200}	Derived from [36,37]
	B	m	Spacing between BHEs	{5,7,10,15,20,25, 30,40,50,70,100}	Derived from H_{max}[25]
Optimisation constraints	q_{nom}	W/m	Nominal heat extraction rate	30 – 45 (41.5)	SIA norm [34]
	H_{max}	m	Maximum borehole depth	Permitted: 200 Limited: 150	Derived from [36,37]
Outputs	N_B	−	Number of boreholes per field	$f(B)$	Section 2.2
	Q_{field}	Wh	Extractable energy of BHE field	$f(H,B)$	Eq. (2), Section 2.2
	H_{opt}, B_{opt}	m	Optimal borehole depth, spacing	$\in H,B$	Section 2.3
	Q_{pot}	Wh	Technical potential	$Q_{field}(H_{opt}, B_{opt})$	Eq. 9, Section 2.3

$$q_{max} = \frac{T_g\left(\frac{H}{2}\right) - T_{mf,min}}{\overline{w}\left(R_{LT}(r_b,H) + R_{field}(B,H)\right) + w_{seas}R_{seas} + R_b} \tag{3}$$

where T_g is given in Eq. (1); $T_{mf,min}$ is constant (Table 1); $\overline{w}$ is the annual mean load of the GSHP system (as fraction of the full load), and is given by $\overline{w} = t_{op}/(365 \times 24\ h)$; R_{LT} is the long-term thermal resistance of a BHE (Appendix A), computed at the borehole wall, i.e. at a radial distance r_b (Table 1); R_{field} (Eq. (4)) is the average long-term thermal resistance of a BHE field; w_{seas} (Eq. (5)) and R_{seas} (Appendix A) are the seasonal mean system load and the seasonal thermal resistance, respectively; and R_b, the borehole thermal resistance, is constant (Table 1). The expressions for R_{LT} and R_{seas}, which depend on λ and α, are provided in Appendix A.

According to the superposition principle [35], the long-term thermal resistance of BHEs in a field may be estimated by summing the R_{LT} at each $r_{i,B} \leq H$, where $r_{i,B}$ is the distance to the i^{th} nearby BHE for a scenario B. For any $r > H$, there is a negligible effect on the thermal response [25]. The R_{field} is the average thermal resistance for N_B BHEs in a field, given by:

$$R_{field}(H,B) = \frac{1}{N_B}\sum_{i=1}^{N_B}\sum_{r_{i,B}\leq H} R_{LT}(r_{i,B},H) \tag{4}$$

To limit the number of possible combinations of B and H, we assume that the BHE spacing and depth within a field equals that of all neighboring fields within a radius of H. We further assume the ground data to be constant within each field, which holds for over 99% of the cases.

The effect of the seasonal variation of the GSHP system load on q_{max} is modelled as the maximum of a sinusoidal heat extraction with a periodicity of 1 year and an amplitude w_{seas} (cf [25]). We derive w_{seas} from the Heating Degree Days (HDD) describing the monthly heating profile of a given location. As Fig. 3 shows, the monthly mean GSHP system load $\overline{w}_m$ (blue bars, as fraction of the full load), weighted by the HDD, resembles a sinusoid superimposed on $\overline{w}$ (red line). We thus propose here to approximate w_{seas} by subtracting $\overline{w}$ from the mean system load in the month with the maximum heating demand (typically January in Switzerland):

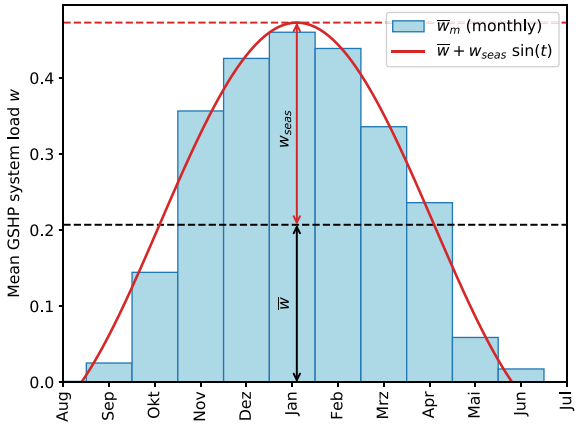

Fig. 3. Example of the monthly mean GSHP system load ($\overline{w}$, blue bars, as fraction of the full load) and its sinusoidal approximation ($\overline{w} + w_{seas}\sin(t)$, red line), based on the HDD of a representative location for western Switzerland (weather station of Pully) with a heating season of ~ 6 months. (For interpretation of the references to colour in this figure legend, the reader is referred to the Web version of this article.)

$$w_{seas} = w_{hdd,max} \times \frac{t_{op}}{31 \times 24h} - \overline{w} \tag{5}$$

where $w_{hdd,max}$ is the highest relative HDD, defined as:

$$w_{hdd,max} = 1.05\frac{HDD_{max}}{\sum HDD} \tag{6}$$

HDD_{max} is the maximum monthly HDD, $\sum HDD$ is the annual sum, and a buffer of 5% (hence the factor 1.05) is multiplied with this ratio to avoid an underestimation of $w_{hdd,max}$. The computation of the HDD from the ambient air temperature is detailed in Appendix B.

2.3. Optimisation

The aim of the optimisation is to select, for each BHE field separately, the borehole density B_{opt} and borehole depth H_{opt} that

maximise Q_{field}, yielding the technical potential Q_{pot}. This optimisation is constrained by two factors: the maximum BHE depth H_{max} and the minimum heat extraction rate q_{min}. The H_{max} is limited by local conditions and regulations (see Section 3.2). The q_{min} represents a proxy of the economic feasibility of a GSHP system. We propose to derive q_{min} from the nominal heat extraction rate q_{nom}, which represents current installation practices. Using the data provided in the SIA norm, q_{nom} can be approximated as [34]:

$$q_{nom} \approx \frac{T_g - T_{mf,min}}{11.5} \left(10.6\lambda + 11.2 + 2\left(\frac{\lambda}{\alpha} - 2\right)\right) \quad (7)$$

To soften this constraint, we set q_{min} at 80% of q_{nom}, which corresponds to the expected power loss for domestic installations with multiple BHEs under the given operating conditions [34]. The optimisation problem may hence be formulated as:

$$Q_{pot} = \max_{B,H} Q_{field} \quad \text{subject to } H \leq H_{max},\ q_{max} \geq 0.8\, q_{nom} \quad (8)$$

3. Case study

To demonstrate the performance of the proposed method at regional scale, we apply it to the cantons of Vaud and Geneva in Switzerland. The selected cantons are well-suited for this study as they consist of both urban and rural zones, already contain a large number of BHEs and offer high-resolution landscape data as well as geothermal cadastres with information for the planning of GSHP systems. Furthermore, the annual heat demand for the cantons is available from Schneider et al. [40] at a pixel resolution of $200 \times 200\ m^2$. This data is used to assess potential surpluses or deficits of geothermal heat generation. For this assessment, we assume that all GSHPs are sized appropriately and have a coefficient of performance (COP) of 4.5 as suggested by Galgaro et al. [20].

The case study covers a surface of around $1600\ km^2$ in the western part of the Swiss plateau that contains over 250,000 buildings. Its largest cities are Geneva and Lausanne at the borders of Lake Geneva (see Fig. 4a). Geologically, the plateau is situated in the alpine Molasse Basin between the Jura in the north and the Prealps in the south. Its shallow subsurface (<400 m) consists primarily of a layer of unconsolidated Quarternary deposits, with a thickness of $0-150$ m, which is located on top of the clastic sedimentary rocks of the Swiss molasse [41].

3.1. Landscape data

The TLM used in this work is obtained from the Swiss Office of Topography (swisstopo) [42] and contains a detailed 3D representation of various landscape objects in vector form. It has an accuracy of $0.2-1.5$ m for well-defined objects such as roads or buildings, and of $1-3$ m for other landscape features such as forests [42]. To account for the inaccuracies of the TLM, we apply a tolerance buffer of 1 m to all objects listed in Section 2.1. Additionally, roads and railways are buffered by their widths. The parcel boundaries are vector representations of the official mensuration data for around 100,000 property units, obtained from the cantonal geoinformation services of Vaud (ASIT-VD) [43] and Geneva (SITG) [44].

3.2. Ground data

The geothermal cadastres, provided by ASIT-VD [36] and SITG [37], contain information on (i) restriction zones for geothermal installations within the case study area, (ii) thermal ground properties, and (iii) over 4400 existing installations with $\sim 10,800$ BHEs. The restriction zones are divided into three categories, shown in Fig. 4a, which indicate whether the installation of BHEs is permitted, limited, or prohibited. Prohibited zones are excluded from the study. The permitted and limited zones are overlaid with information from existing installations to derive H_{max}, as no data on the allowed drilling depth is available. Based on these considerations, we choose H_{max} as the 75th percentile of the depth of the existing BHEs, yielding values of $200m$ and 150 m for the "permitted" and "limited" zones, respectively.

The ground data provided in the cadastres include the thermal conductivity (λ) and the heat capacity (ρC, Geneva only), from which the diffusivity is obtained as $\alpha = \lambda/\rho C$ [25]. The λ and ρC are computed as the average of the ground properties of each rock layer weighted by its thickness, which is given by 3D models of the subsurface [45]. The ground data exists for depths in the range of $50-300$ m as pixels of 50 m spatial resolution in all 3 dimensions. Constrained by this spatial resolution and H_{max}, we obtain four scenarios for the borehole depth H (see Table 1). To obtain λ and ρC for all scenarios of H in the entire study region, we compute any missing values as weighted averages using tabulated data [34,45]. The resulting maps for λ and α for a borehole depth of $H = 100$ m are shown in Fig. 4c and d.

The data for T_0 has been provided by Assouline et al. [16] for pixels of 200 m resolution. The data is estimated from ground measurements using Machine Learning [16]. To minimise the impact of the built environment on these measurements, we use the annual average ground temperature at a depth of 1 m. Its interpolated values at the resolution of λ and α is shown in Fig. 4b. The temperature gradient in the Swiss plateau is approximately constant at $0.03 K/m$ [34].

4. Results

4.1. Available area and borehole fields

The application of our method to the case study region in western Switzerland suggests that an area of $284\ km^2$ may be available for the installation of BHEs on 80,000 of the 100,000 parcels (property units). The percentage of available area varies widely within the case study region, as the aggregation of the parcels to pixels of $200 \times 200\ m^2$ shows (Fig. 5). The available area is small in dense urban areas, particularly at the borders of Lake Geneva, and drops below 10% in the city centers of Lausanne and Geneva. In rural areas, the spread is much larger, varying widely between nearly 0% and 100%. This is due to the fact that rural parcels are spaced far apart and may cover multiple pixels.

The results yield BHE fields for each density scenario B (see Table 1), an example of which ($B = 7$ m) is shown in Fig. 6a. This scenario equals the current recommendations for the distance between BHEs [6], but it results in unrealistically high numbers of BHEs in large fields. Borehole spacings of around $H/2$ ($B = 50-100$ m), on the other hand, represent conservative scenarios that leave many fields unused.

4.2. Thermal resistance of interacting boreholes

The simulation results show that the thermal resistance R_{field}, representing the interactions between boreholes, varies with the parcel shape and size. As the thermal resistance decreases logarithmically with distance to a borehole, the average R_{field} is strongly influenced by the average number of immediately neighboring BHEs within a parcel. Consequently, large fields have a higher R_{field} than small or oddly shaped ones (see colour gradient in Fig. 6a for $B = 7$ m, $H = 50$ m). In particular, R_{field} is small in fields located next to roads or other unavailable areas, where no BHEs can be

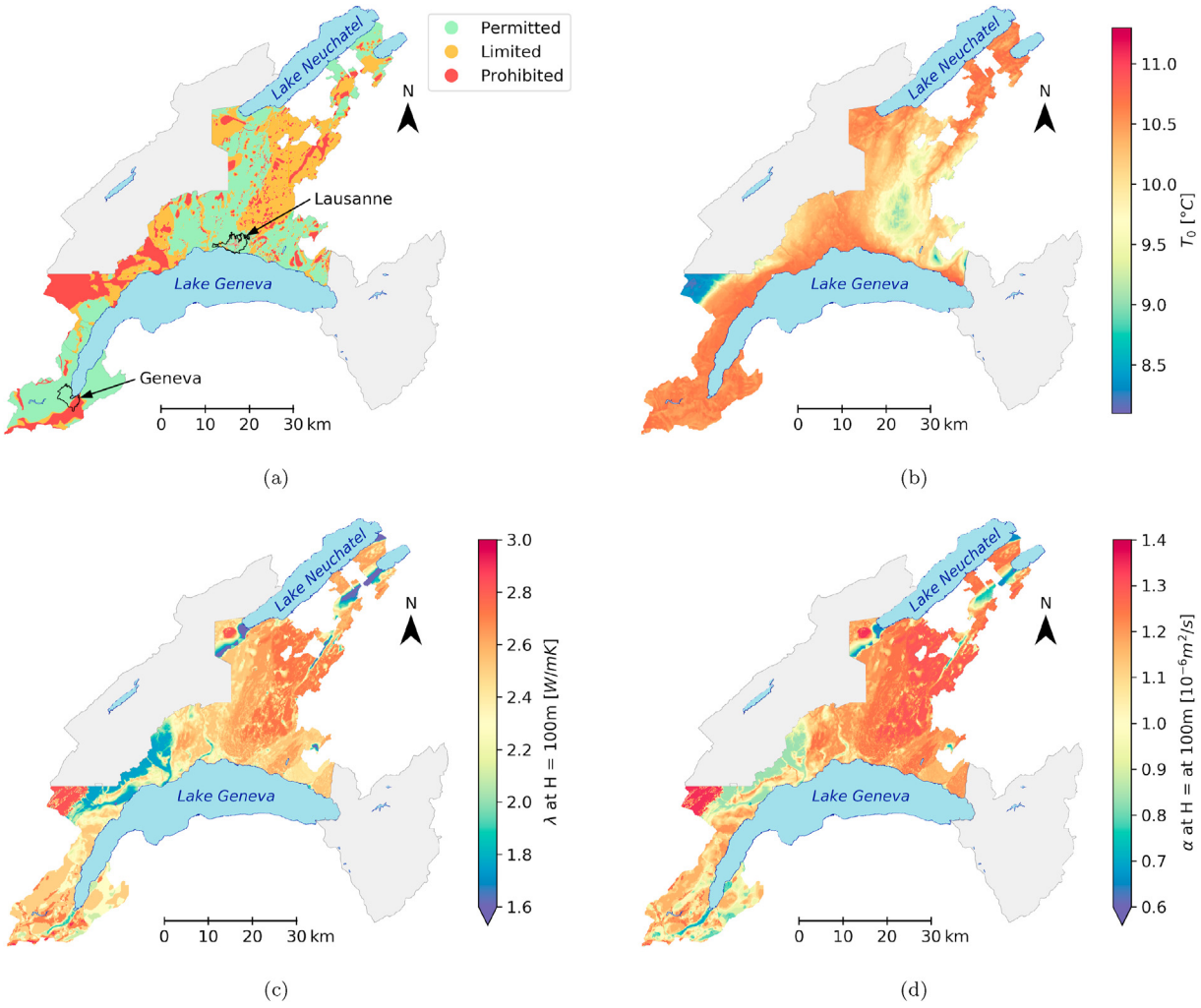

Fig. 4. Regional variation of ground data in the case study region. a) Restriction zones for geothermal installations, b) Ground surface temperature at $1m$ depth, obtained from Assouline et al. [16], c) Thermal conductivity (λ) and d) Thermal diffusivity (α) derived from the geothermal cadastres [37,43]. Grey zones are outside the study area.

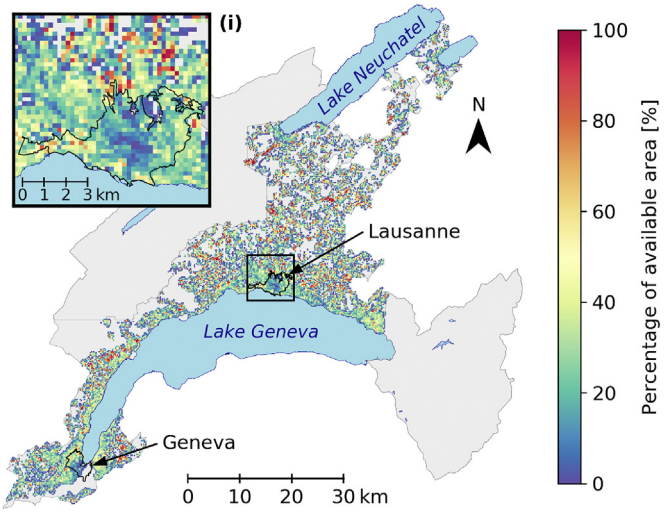

Fig. 5. Percentage of available area for pixels of $200 \times 200m^2$, obtained as the sum of the available area of all parcels within a pixel, relative to the pixel area of $40,000m^2$. The inset (i) shows a zoom into the area around Lausanne.

installed (white spaces in Fig. 6a). The relationship between R_{field} and the borehole spacing also causes R_{field} to fall steeply as B increases, for any H (see Fig. 6b). Fig. 6b further shows that R_{field} increases non-linearly with H, which means that decreasing H reduces interactions between BHEs. For H = 50 m, R_{field} drops below the long-term resistance of the BHE itself (R_{LT}, dashed line) near B = 11.5 m, at which point the field resistance is no longer dominating the long-term effects, and flattens out near B = 25 m. The same behaviour is found for H ≥ 100 m, but at spacings of 20 m and 50 m, respectively.

4.3. Optimisation and trade-offs

The optimisation yielding the technical potential Q_{pot} requires a trade-off between the heat extraction rate q_{max} and the extractable energy Q_{field}, which is shown in Fig. 7. It indicates that q_{max} (Fig. 7a) increases with borehole spacing B for all borehole depths H, while Q_{field} (Fig. 7b) decreases with B due to a lower number of installed BHEs (N_B). Notably, q_{max} decreases with H for low B, but shows the opposite behaviour if B is high. The former is due to the lower R_{field} of shallower BHEs (see Fig. 6b), while the latter is driven by a higher ground temperature at higher depths. The intersection of q_{max} with the thresholds of 80% of q_{nom} (dashed lines in Fig. 7a) suggests that the average B_{opt} (dots) lies between 10 – 20 m, very close to the

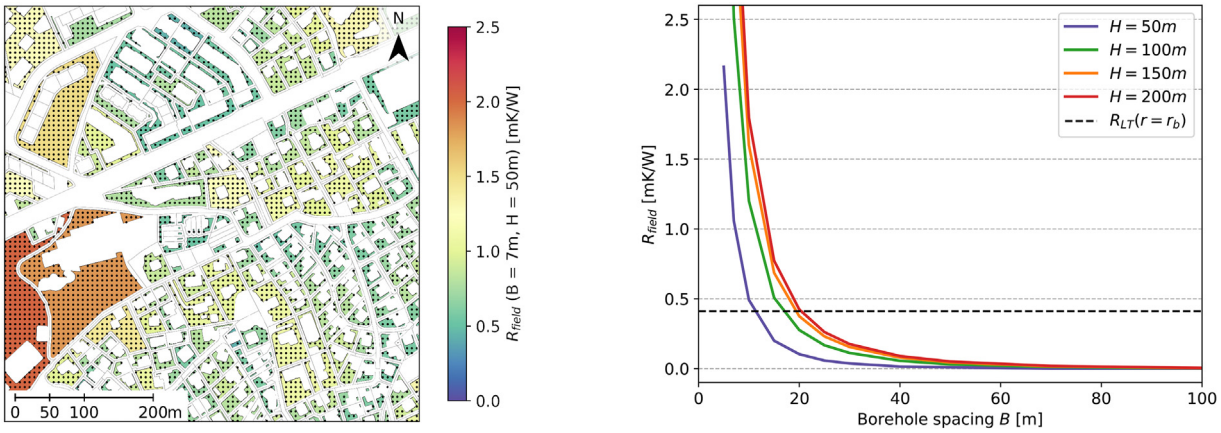

Fig. 6. a) Sample of borehole fields for a suburban area near Geneva, showing the potential BHEs for $B = 7m$ (black dots) and the corresponding thermal resistance R_{field} (colour gradient) at $H = 50m$, b) R_{field} for each scenario of B and H, averaged across all fields. The dashed line indicates the long-term resistance at the borehole wall ($R_{LT}(r = r_b)$), averaged for all H. (For interpretation of the references to colour in this figure legend, the reader is referred to the Web version of this article.)

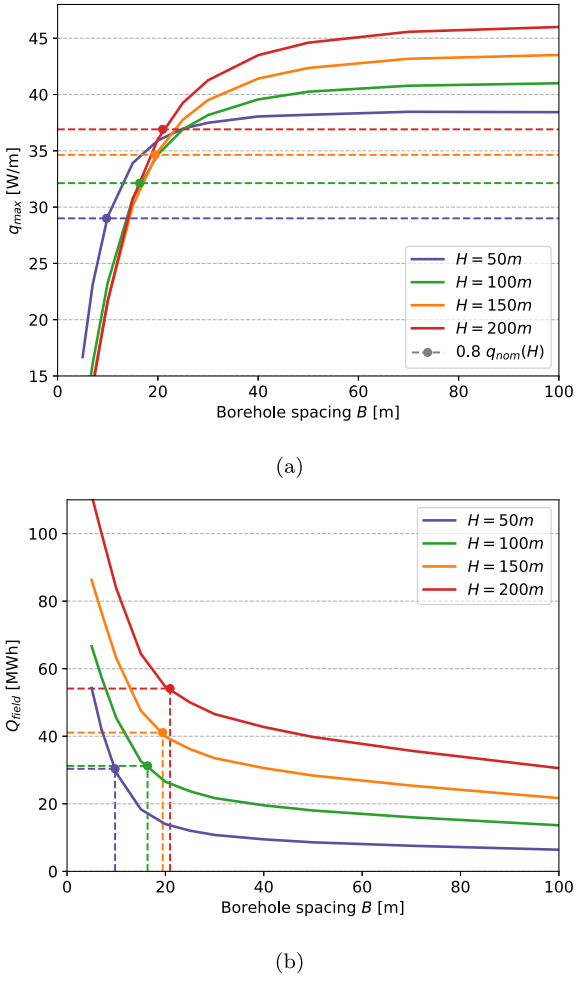

Fig. 7. Heat extraction rate q_{max} (a) and the corresponding extractable energy Q_{field} (b) as a function of B and H. The lines show averages across 90% of the fields, excluding the lowest and highest 5^{th} percentile. The dots in both figures indicate the intersection of q_{max} with 0.8 q_{nom}, the minimum accepted operating power for each H shown as dashed line in (a).

intersections of R_{field} with R_{LT} (see Fig. 6b). The higher q_{max} for low H may in some cases outweigh the greater BHE depth, as the lower R_{field} of shallow BHEs allows for a lower B. On average, this yields an equal potential for H = 50 m and H = 100 m, and it may result in $H_{opt} < H_{max}$ in the optimisation.

The B_{opt} and H_{opt} resulting from the optimisation are shown in Fig. 8, averaged for each pixel of 200 × 200 m^2. The average B_{opt} ranges from 5 – 10 m in urban areas to 30 – 40 m in rural areas, where many large fields are located. As large fields have, on average, a higher R_{field} than small fields (see Fig. 6a), a higher spacing B_{opt} is required to fulfill the optimisation constraints. The H_{opt} is close to the maximum value of 200 m in the "permitted" zone but varies between 50 – 150 m in the "limited" areas. As H_{max} = 150 m in the "limited" zone, the benefits of a relatively high q_{max} frequently outweigh the additional energy gain from a higher H (see Fig. 7).

The results further indicate that the optimal number of installed BHEs ($N_{B,opt}$, i.e. N_B at $B = B_{opt}$) decreases with H_{opt}, as deeper BHEs frequently require a higher spacing to fulfil the optimisation constraints. As Fig. 9 shows, the maximum $N_{B,opt}$ (blue line) decreases from 40 BHEs per hectare (corresponding to an average B_{opt} of 15 m) for the shortest probes to 10 BHEs (B_{opt} = 30 m) for H_{opt} = 200 m. By contrast, the maximum cumulative BHE depth per hectare (red line) is approximately constant with H_{opt}, at just below 2 km/ha given a minimum borehole spacing of 5 m and a maximum depth of 200 m. These findings suggest that the cumulative installed borehole depth per hectare may more suitable for constraining the dense deployment of BHEs than a minimum spacing between adjacent boreholes.

4.4. Technical geothermal potential

The technical potential (Fig. 10) yields an annual total of 4.65 *TWh* for all parcels, or 16.4 kWh/m^2 of available area (284 k m^2). Most of the parcels (∼ 60%) are fitted with one or two BHEs, frequently in gardens of private properties (see Fig. 10a). Those of a shallow depth (≤ 100 m) yield less than 15 MWh, while deeper BHEs, ≥ 150 m, may provide up to 35 MWh per field. How boreholes are arranged in larger fields (> 2 BHEs) depends on the shapes and sizes of the fields. For example, narrow fields have a small thermal influence from adjacent BHEs, which results in a maximum potential for shallow and closely spaced (here 10 m)

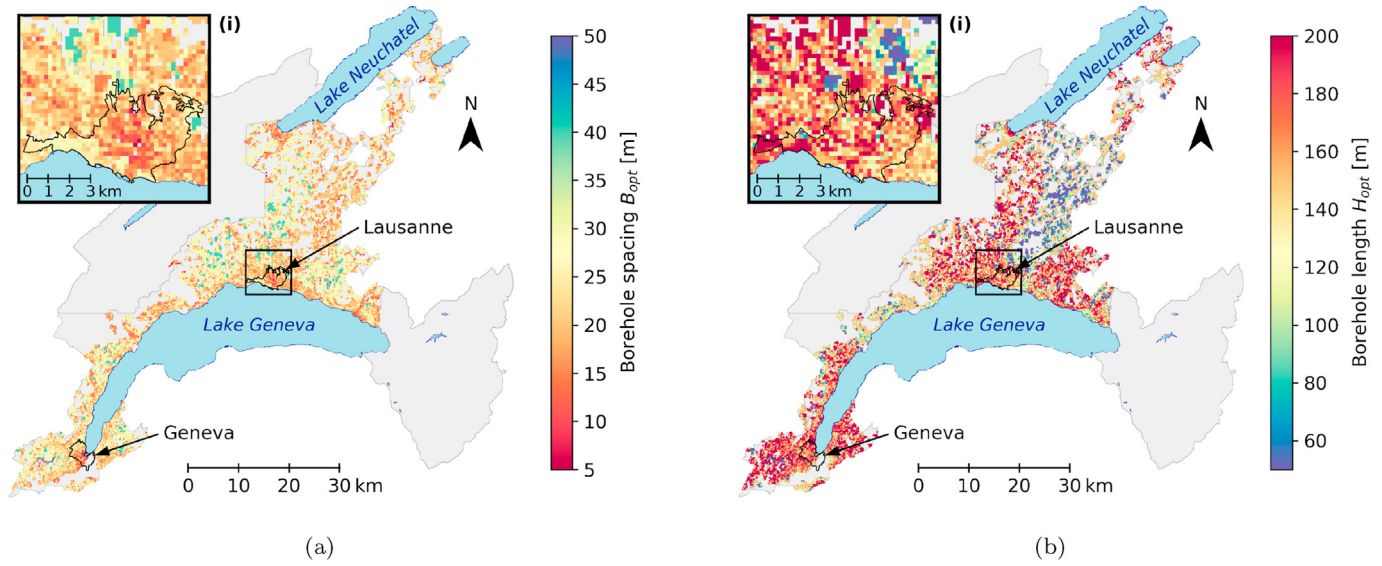

Fig. 8. a) Optimised borehole spacing B_{opt} and b) borehole depth H_{opt}, both averaged across all BHEs within each 200 × 200m^2 pixel. The value for B_{opt} accounts only for those fields with more than one BHE and represents the average per available area.

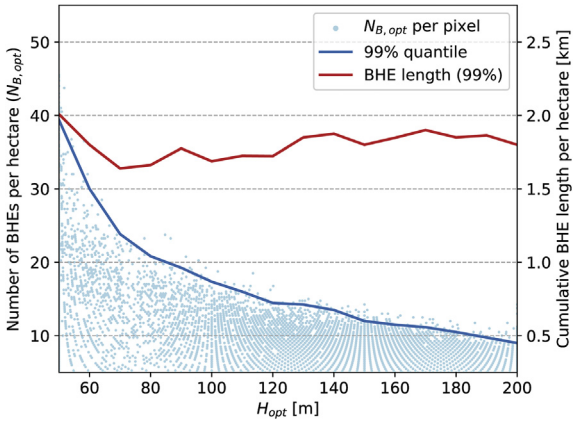

Fig. 9. Optimal number of boreholes ($N_{B,opt}$) per hectare for all 200× 200m^2 pixels (dots). The blue line marks the 99th percentile per average depth H_{opt} (10m bins). The red line shows the corresponding cumulative installed BHE depth, given by $N_{B,opt}$ × H_{opt} (right axis). The normalization per hectare is chosen for reasons of interpretability. (For interpretation of the references to colour in this figure legend, the reader is referred to the Web version of this article.)

boreholes. The influence of surrounding BHEs is highest for fields of rectangular shape, leading to a larger spacing (here 30 m) and the maximum depth. Few parcels (∼ 2%) are very large and may fit more than 60 BHEs, which exceeds the maximum existing field size in the region. If all fields are capped to this value, the annual potential reduces to 4 TWh.

The variation of the energy density, defined as the technical potential per unit area (Fig. 10b), ranges from 2 kWh/m^2 to 15.5 kWh/m^2. The highest energy density is found in the urban and suburban areas at the borders of the lakes of Geneva and Neuchâtel (∼ 30% of available area) and in rural areas with an available area percentage near 100%. In the city centers of Lausanne and Geneva, the energy density is low despite the high H and low B, as the available area is small (< 10%). Furthermore, the area in the north-east of Lausanne is characterised by a lower potential. This zone has a lower surface temperature (see Fig. 4b), which reduces the total allowed temperature drop.

In contrast to the technical potential, the energy demand is strongly concentrated in urban areas and exceeds 1 MWh/m^2 in the centers of Lausanne and Geneva, as shown in Fig. 11a. This leads to a large local energy deficit in these areas (Fig. 11b), where complementary sources of renewable heat are indispensable. In most rural areas, however, the energy demand can be covered fully by the geothermal potential, and partially excess generation may be possible.

4.5. Sensitivity analysis

The sensitivity analysis of the main input parameters (λ, α, T_0, $\delta T/\delta z$, t_{op}, r_b, R_b) suggests that the energy potential of individual fields is, on average, most sensitive to T_0 and λ, followed by t_{op} and R_b (see Fig. 12a). Accounting for the regional variation of these parameters (except R_b) with the highest possible accuracy is thus essential for a realistic potential estimate. Furthermore, the estimation is sensitive to uncertainties in these values, which may arise from small-scale deviations and measurement errors, as well as from parameter variations due to different technologies and operation strategies. The sensitivity of α, r_b and $\delta T/\delta z$ is low, so the use of standard values from the literature is justified.

The results are exploratory and aim at providing an indication of the importance of each parameter on the technical potential. The change in Q_{field} is obtained by varying each parameter separately around the average input data (see Table 1) and for the average BHE arrangement (H = 150 m, B = 20 m, 8 neighboring boreholes). While Fig. 12a shows the average sensitivity of Q_{field} in the context of this case study, the results depend on the exact borehole arrangements and operation strategies.

The technical potential of GSHPs is further sensitive to the selected optimisation constraints, namely q_{min} (percentage of q_{nom}) and H_{max}. As Fig. 12b shows, the total technical potential decreases linearly with q_{min} and increases over-proportionally with H_{max}, following the results from Fig. 7. The Q_{pot} may hence be increased by accepting a lower minimum operating power or by increasing the maximum drilling depth. Doubling the potential for the given H_{max} (dashed line in Fig. 12b) would for example require dropping q_{min} to only 50% of q_{nom}. Notably, the impact of H_{max} on Q_{pot} decreases with q_{min} and becomes insignificant when $q_{min} = q_{nom}$, as

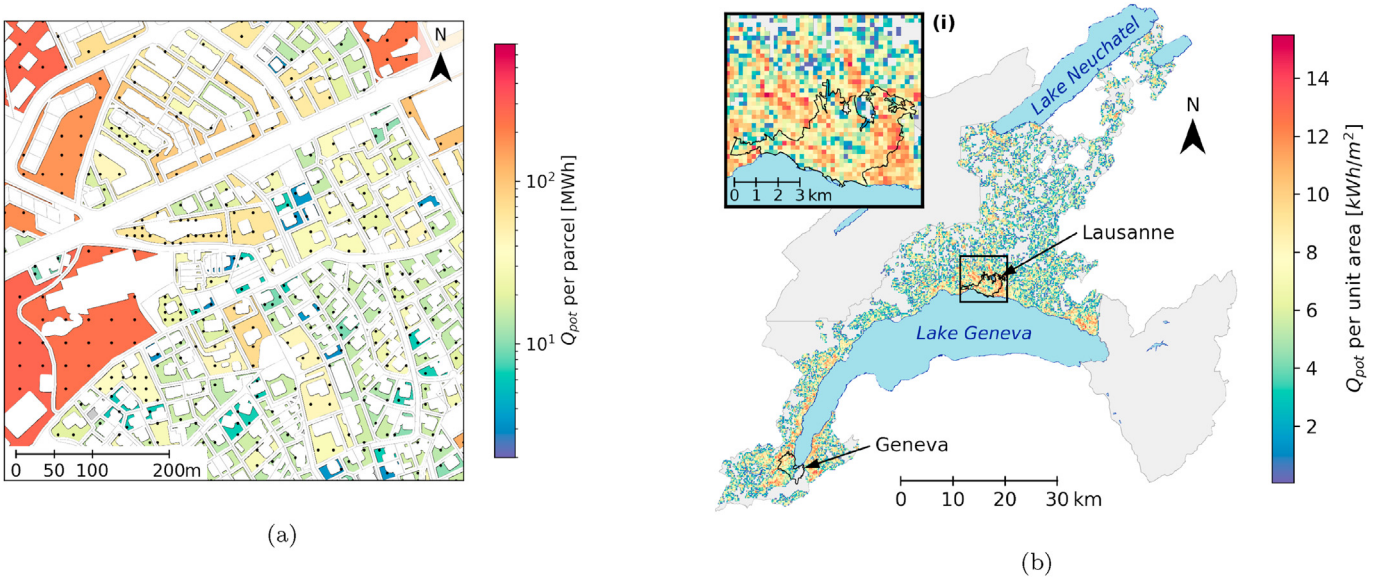

Fig. 10. a) Annual technical potential Q_{pot} (in *MWh*) for the sample area (coloured fields), with the optimised BHE locations (dots), b) Q_{pot} per unit area (in $kWh/\ m^2$) for pixels of $200 \times 200m^2$.

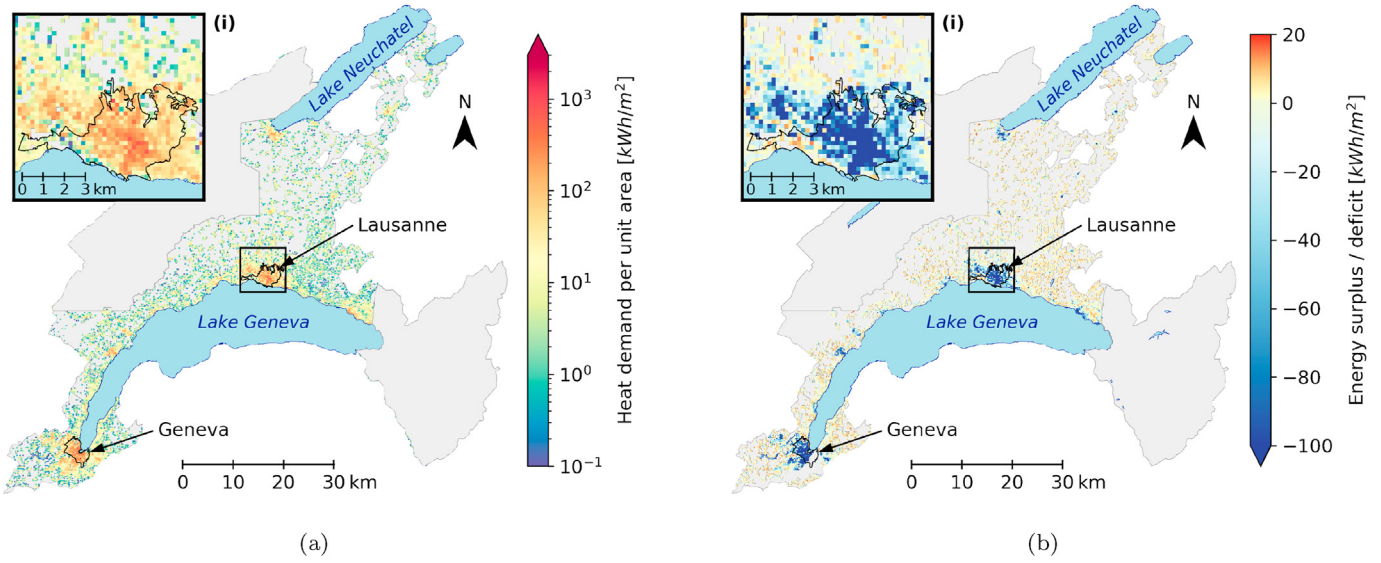

Fig. 11. a) Annual heat demand density (logarithmic scale) for pixels of $200 \times 200m^2$, according to Schneider et al. [40], b) Surplus (positive) or deficit (negative) of potential heat extraction from BHEs compared to the heat demand.

the BHE arrangements converge to H = 50 m, B = 25 m beyond 100% of q_{nom}.

5. Discussion

5.1. Methodological contribution

Here we propose a novel approach for estimating the technical potential of GSHPs at regional scale, taking into account the available area for the installation of BHEs as well as the thermal interactions between boreholes. The strength of our method lies in the combination of GIS and analytical modelling to simulate the potential effects of a dense deployment of BHEs for multiple scenarios of borehole spacing and depth. As we derive the energy potential for each scenario from the maximum operating power under current installation standards, the estimation is independent of the energy demand. The scenarios provide insights into the trade-off between energy and operating power, which is exploited in an optimisation step to suggest an optimised arrangement of BHEs for each individual parcel. The spatial resolution of individual parcels allows to assess the impact of parcel shape, size and location on the technical potential, while the regional scale of the study highlights variations of the technical potential in urban and rural areas.

5.2. Practical implications

The case study in western Switzerland yields several practical contributions for a potential dense deployment of geothermal heat pumps. Firstly, we provide a regional-scale dataset of a technical

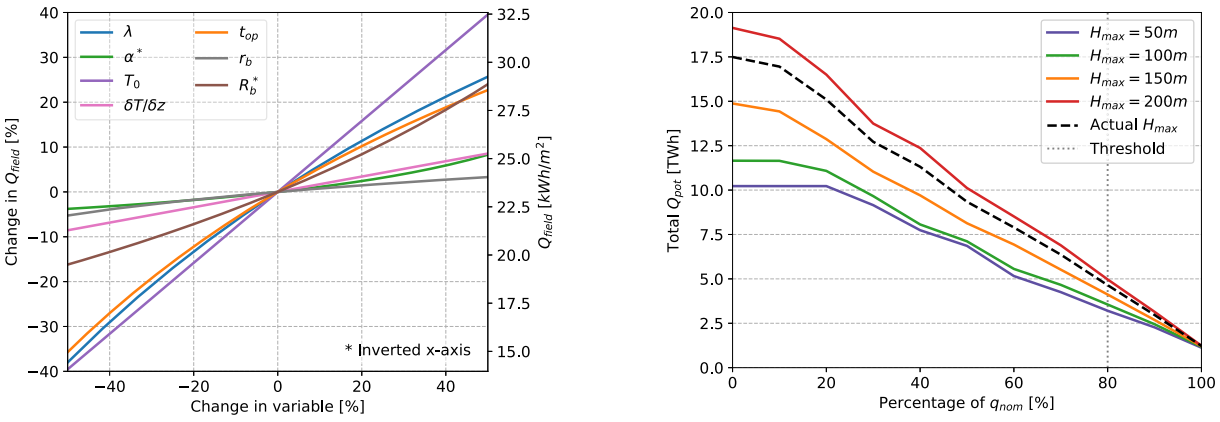

(a) (b)

Fig. 12. a) Sensitivity of Q_{field} to changes in the ground data (λ, α, T_0, $\delta T/\delta z$) and the technical parameters (t_{op}, r_b, R_b). The change in Q_{field} is computed by varying each parameter around the average values in Table 1 for the average BHE arrangement of $H = 150m$, $B = 20m$ and 8 neighboring boreholes. b) Sensitivity of the technical potential Q_{pot} to changes in the required heat extraction rate (x-axis) and in H_{max} (colours), summed across all fields. The dashed line shows the varying H_{max} used here. (For interpretation of the references to colour in this figure legend, the reader is referred to the Web version of this article.)

potential of GSHPs that accounts for interactions between boreholes and yields a potential of 4.65 TWh on an available area of 284 km^2. Secondly, the aggregation to pixels of 200× 200 m^2 highlights regional variations in the potential, which reaches up to 15.5 kWh/m^2. According to our estimation, the potential is great enough to satisfy the heating demands in most rural and suburban areas but it is insufficient in urban centers, where complementary heat supplies would be needed. Thirdly, our analysis suggests that the cumulative installed borehole depth is a good indicator for the exploitation of the thermal capacity of the ground. In this case study, which assures at least 80% of the nominal operating power for potential installations, the upper limit of cumulative depth is about 2 km/ha given a minimum borehole spacing of 5 m and a maximum depth of 200 m.

5.3. Limitations

As any study estimating a technical potential of GSHPs, the present work is subject to uncertainties related to the modelling approach and the data. The primary source of uncertainty is related to the ground thermal properties (λ, α), as the underlying 3D subsurface models are regional models and may deviate from measured thermal properties in some locations. Such local deviations can only be assessed through test drillings.

This work is limited by some assumptions: (i) the entire available area is considered suitable for installing BHEs. In practice, alternative uses of the subsurface such as utility lines, subways or tunnels may reduce the available area for geothermal installations [46]. (ii) All BHE arrangements are based on rectangular grids covering the full area. The BHE arrangements suggest borehole numbers and depths that maximise the energy potential in the context of a dense deployment of BHEs, and do not represent installation recommendations for specific parcels. (iii) We focus on the technical aspects limiting a dense deployment of BHEs. Other aspects, such as environmental consequences due to cooling of the shallow subsurface, are not addressed here. (iv) We do not consider additional heat transfer from groundwater flow, which may impact the technical geothermal potential. (v) More specifically, we only consider heat extraction for space heating, which is the dominant use of GSHPs in Switzerland. The estimated potential may increase if excess heat, for example from space cooling, is re-injected into the ground, as that would partly recharge the ground with heat. For countries with similar yearly temperatures as Switzerland or lower, the amount of heat re-injected into the ground during the comparatively short hot summer periods is likely to be small in relation to the heat extracted from the ground during the much longer cool winter periods. The details of this impact will be explored in a future work.

As this work is, to the best of our knowledge, the first of its kind in the case study area, a frame of comparison is lacking. While the quality of the ground data may be assessed from thermal response tests, a validation of the thermal interference between boreholes is only possible for individual case studies that already exhibit a high density of BHEs. The relevance of such a validation approach however is limited, as real installations are dimensioned to satisfy a given demand, while this work is aimed at estimating the maximum possible energy generation.

5.4. Applications and future work

Applications for a regional-scale estimate of the technical potential of BHEs include the support of policy making, urban planning and the development of a framework for the regulation of new installations. As part of their renewable energy strategies, policy makers may provide financial support mechanisms for businesses, homeowners and energy providers to invest in GSHPs, knowing that these may cover significant fractions of the heat demand in suburban and rural areas.

Urban planners can use the results (i) to estimate the potential of GSHPs in any neighborhood in the study region, (ii) to assess the potential of district heating networks for transporting heat from areas with surplus generation to those with a deficit and/or (iii) to perform techno-economic analyses that compare GSHPs to alternative heat sources. Local authorities may use the outcome from the proposed method to explore the limiting factors for a dense deployment of BHEs and to formulate guidelines to avoid an over-exploitation of the ground.

Future work will aim at the estimation of a technical geothermal potential at country scale. This may be achieved by applying statistical methods such as Machine Learning, which have been used successfully to estimate the theoretical geothermal potential at national scale [16]. To further develop the proposed method, several limitations may be addressed, including the modelling of the additional heat transfer from groundwater flow, a systematic

quantification of the uncertainties related to the data and the modelling approach and the impact of an active regeneration of the ground on the geothermal potential in dense urban areas.

6. Conclusion

This work presents an estimation of the technical geothermal potential from shallow ground-source heat pumps for individual parcels at regional scale. We define the technical potential as the maximum thermal energy that can be extracted from vertical borehole heat exchangers installed on all the available surface area, such that these can be operated with at least 80% of the recommended operating power. The proposed method combines the ground thermal properties, the available area for borehole installation and the technical model of borehole heat exchangers and focuses on quantifying the thermal interference between boreholes, which has not previously been assessed at the regional scale.

The results provide a first estimate of the technical potential of borehole heat exchangers for a case study area in western Switzerland. This estimate suggests that borehole heat exchangers may provide sufficient energy to cover the heat demand of most suburban and rural areas, while the potential is insufficient in dense urban centers. Urban planners can use this data to assess the techno-economic aspects of a dense deployment of borehole heat exchangers. Our findings further show that the cumulative installed borehole depth may be a suitable parameter to assess a potential over-exploitation of the heat capacity of the ground. This work can contribute to the development of decarbonisation strategies for the heating sector in Switzerland by quantifying the potential for a renewable heat generation from shallow geothermal energy and by highlighting areas where complementary heat sources are needed.

CRediT authorship contribution statement

Alina Walch: Conceptualization, Methodology, Software, Visualization, Writing - original draft. **Nahid Mohajeri:** Conceptualization, Writing - review & editing, Supervision, Funding acquisition. **Agust Gudmundsson:** Writing - review & editing. **Jean-Louis Scartezzini:** Supervision, Project administration, Funding acquisition.

Declaration of competing interest

The authors declare that they have no known competing financial interests or personal relationships that could have appeared to influence the work reported in this paper.

Acknowledgements

We thank the reviewers and the editor for very thorough reviews and helpful comments on an earlier version of this article. This research has been financed partly by the Swiss National Science Foundation (SNSF) under the National Research Program 75 (Big Data) for HyEnergy project, No. 407540_1167285, and partly by the Swiss Innovation Agency Innosuisse under the Swiss Competence Center for Energy Research SCCER FEEB&D.

Appendix A. Analytical models for thermal resistance

This section provides the formulas for the long-term and seasonal thermal resistance used in this work, based on the data from Table 1. For details regarding the underlying analytical models, please refer to Ref. [25]. For the long-term thermal resistance (R_{LT}) we apply the finite line source (FLS) model, which is commonly used to simulate interactions of BHEs [5,6]. To compute the mean R_{LT} along the borehole length at a radial distance r from the BHE, we have implemented an efficient solution for the integration of the FLS model along the vertical axis proposed in Ref. [47]:

$$R_{LT}(r,H) = \frac{1}{4\pi\lambda} \int_{\frac{1}{\sqrt{4at}}}^{\infty} e^{-r^2 s^2} \frac{I_{ls}(Hs,Ds)}{Hs^2} ds \tag{A.1}$$

where

$$I_{ls}(h,d) = 2\,\mathrm{ierf}(h) + 2\,\mathrm{ierf}(h+2d) - \mathrm{ierf}(2h+2d) - \mathrm{ierf}(2d)$$

$$\mathrm{ierf}(x) = \int_0^x \mathrm{erf}(u)du = x\,\mathrm{erf}(x) - \frac{1}{\sqrt{\pi}}\left(1 - e^{-x^2}\right)$$

$$\mathrm{erf}(x) = \frac{2}{\sqrt{\pi}} \int_0^x e^{-\mu^2} d\mu$$

and t equals the planning horizon t_{dim}. D is the distance between the BHE outlet and the ground surface, which is set to D = 2 m as suggested in Ref. [25]. To compute R_{LT} for many BHE fields with large numbers of BHEs, the integrand in Eq. (A.1) has been precomputed for all combinations of α and r, exploiting the geometrical properties of the BHE arrangement in grids.

The maximum of the seasonal thermal resistance (R_{seas}) at the borehole wall ($r = r_b$), modelled as sinusoidal heat extraction with a period (t_{seas}) of one year, is given by Ref. [48]:

$$R_{seas} = \frac{1}{2\pi\lambda} \sqrt{\left(\ln\left(2/r_{pb}'\right) - \gamma\right)^2 + \pi^2/16} \tag{A.2}$$

where

$$r_{pb}' = r_b\sqrt{2}/\delta < 0.1$$

$$\delta = \sqrt{\alpha t_{seas}/\pi}$$

and γ is Euler's constant (0.57221…) and δ is the penetration depth. As δ lies below B_{min}, R_{seas} is independent from surrounding BHEs.

Appendix B. Heating degree days (HDD)

The HDD is defined in the norm SIA 2028 as the sum of the heating degrees for each month m, averaged across 20 years, such that [49]:

$$HDD = \frac{1}{20} \sum_{y=1}^{20} \sum_{d=1}^{d_m} (20 - T_m(d,m,y)) \quad \forall T_m(d,m,y) \leq 12^\circ C. \tag{B.1}$$

where d_m is the number of days of each month and T_m is the daily mean temperature on day d in month m of year y. We use gridded daily temperature data from MeteoSwiss [50] for the years of 1991 – 2011 to compute the monthly HDD, which we spatially interpolate to a resolution of 200 × 200 m^2.

References

[1] C. Bauer, L. Baldini, M. Berger, A. Haselbacher, J. Roth, W. Villasmil, J. Worlitschek, Faktensammlung Wärme. Herkunft und Nutzung in der Schweiz, Technical Report, AEE Suisse, Switzerland, 2019.
[2] F. Stauffer, P. Bayer, P. Blum, N.M. Giraldo, W. Kinzelbach, Thermal Use of Shallow Groundwater, CRC Press, 2013.
[3] G. Florides, S. Kalogirou, Ground heat exchangers—a review of systems, models and applications, Renew. Energy 32 (2007) 2461–2478, https://

doi.org/10.1016/j.renene.2006.12.014.
[4] B. Sanner, C. Karytsas, D. Mendrinos, L. Rybach, Current status of ground source heat pumps and underground thermal energy storage in Europe, Geothermics 32 (2003) 579–588, https://doi.org/10.1016/S0375-6505(03)00060-9.
[5] J.A. Rivera, P. Blum, P. Bayer, Increased ground temperatures in urban areas: estimation of the technical geothermal potential, Renew. Energy 103 (2017) 388–400, https://doi.org/10.1016/j.renene.2016.11.005.
[6] S. Miglani, K. Orehounig, J. Carmeliet, A methodology to calculate long-term shallow geothermal energy potential for an urban neighbourhood, Energy Build. 159 (2018) 462–473, https://doi.org/10.1016/j.enbuild.2017.10.100.
[7] M. Alcaraz, L. Vives, E. Vázquez-Suñé, The T-I-GER method: a graphical alternative to support the design and management of shallow geothermal energy exploitations at the metropolitan scale, Renew. Energy 109 (2017) 213–221, https://doi.org/10.1016/j.renene.2017.03.022.
[8] P. Bayer, G. Attard, P. Blum, K. Menberg, The geothermal potential of cities, Renew. Sustain. Energy Rev. 106 (2019) 17–30, https://doi.org/10.1016/j.rser.2019.02.019.
[9] J. Majorowicz, S.E. Grasby, W.R. Skinner, Estimation of shallow geothermal energy resource in Canada: heat gain and heat sink, Nat. Resour. Res. 18 (2009) 95–108, https://doi.org/10.1007/s11053-009-9090-4.
[10] B. Tian, Y. Kong, Y. Gong, C. Ye, Z. Pang, J. Wang, D. Zhang, An improved volumetric method of geothermal resources assessment for shallow ground combining geophysical data, Renew. Energy 145 (2020) 2306–2315, https://doi.org/10.1016/j.renene.2019.08.005.
[11] D. Bertermann, H. Klug, L. Morper-Busch, A pan-European planning basis for estimating the very shallow geothermal energy potentials, Renew. Energy 75 (2015) 335–347, https://doi.org/10.1016/j.renene.2014.09.033.
[12] A. Gemelli, A. Mancini, S. Longhi, GIS-based energy-economic model of low temperature geothermal resources: a case study in the Italian Marche region, Renew. Energy 36 (2011) 2474–2483, https://doi.org/10.1016/j.renene.2011.02.014.
[13] R. Perego, S. Pera, A. Galgaro, Techno-economic mapping for the improvement of shallow geothermal management in southern Switzerland, Energies 12 (2019) 279, https://doi.org/10.3390/en12020279.
[14] A. García-Gil, E. Vázquez-Suñe, M.M. Alcaraz, A.S. Juan, J.A. Sánchez-Navarro, M. Montlleó, G. Rodríguez, J. Lao, GIS-supported mapping of low-temperature geothermal potential taking groundwater flow into account, Renew. Energy 77 (2015) 268–278, https://doi.org/10.1016/j.renene.2014.11.096.
[15] M. Muñoz, P. Garat, V. Flores-Aqueveque, G. Vargas, S. Rebolledo, S. Sepúlveda, L. Daniele, D. Morata, M.A. Parada, Estimating low-enthalpy geothermal energy potential for district heating in Santiago basin–Chile (33.5°S), Renew. Energy 76 (2015) 186–195, https://doi.org/10.1016/j.renene.2014.11.019.
[16] D. Assouline, N. Mohajeri, A. Gudmundsson, J.-L. Scartezzini, A machine learning approach for mapping the very shallow theoretical geothermal potential, Geoth. Energy 7 (2019) 19, https://doi.org/10.1186/s40517-019-0135-6.
[17] M. Alcaraz, A. García-Gil, E. Vázquez-Suñé, V. Velasco, Advection and dispersion heat transport mechanisms in the quantification of shallow geothermal resources and associated environmental impacts, Sci. Total Environ. 543 (2016) 536–546, https://doi.org/10.1016/j.scitotenv.2015.11.022.
[18] D. Viesi, A. Galgaro, P. Visintainer, L. Crema, GIS-supported evaluation and mapping of the geo-exchange potential for vertical closed-loop systems in an Alpine valley, the case study of Adige Valley (Italy), Geothermics 71 (2018) 70–87, https://doi.org/10.1016/j.geothermics.2017.08.008.
[19] C. Tissen, S.A. Benz, K. Menberg, P. Bayer, P. Blum, Groundwater temperature anomalies in central Europe, Environ. Res. Lett. 14 (2019) 104012, https://doi.org/10.1088/1748-9326/ab4240.
[20] A. Galgaro, E. Di Sipio, G. Teza, E. Destro, M. De Carli, S. Chiesa, A. Zarrella, G. Emmi, A. Manzella, Empirical modeling of maps of geo-exchange potential for shallow geothermal energy at regional scale, Geothermics 57 (2015) 173–184, https://doi.org/10.1016/j.geothermics.2015.06.017.
[21] Y. Noorollahi, H. Gholami Arjenaki, R. Ghasempour, Thermo-economic modeling and GIS-based spatial data analysis of ground source heat pump systems for regional shallow geothermal mapping, Renew. Sustain. Energy Rev. 72 (2017) 648–660, https://doi.org/10.1016/j.rser.2017.01.099.
[22] A. Casasso, R. Sethi, G. POT, A quantitative method for the assessment and mapping of the shallow geothermal potential, Energy 106 (2016) 765–773, https://doi.org/10.1016/j.energy.2016.03.091.
[23] Y. Zhang, R. Choudhary, K. Soga, Influence of GSHP system design parameters on the geothermal application capacity and electricity consumption at city-scale for Westminster, London, Energy Build. 106 (2015) 3–12, https://doi.org/10.1016/j.enbuild.2015.07.065.
[24] K. Schiel, O. Baume, G. Caruso, U. Leopold, GIS-based modelling of shallow geothermal energy potential for CO2 emission mitigation in urban areas, Renew. Energy 86 (2016) 1023–1036, https://doi.org/10.1016/j.renene.2015.09.017.
[25] D. Pahud, Geothermal Energy and Heat Storage, SUPSI Laboratory of Energy, Ecology and Economy, Switzerland, 2002. Technical Report.
[26] G. Stegnar, D. Staničić, M. Česen, J. Čižman, S. Pestotnik, J. Prestor, A. Urbančič, S. Merše, A framework for assessing the technical and economic potential of shallow geothermal energy in individual and district heating systems: a case study of Slovenia, Energy 180 (2019) 405–420, https://doi.org/10.1016/j.energy.2019.05.121.
[27] R. Wagner, T. Weisskopf, Erdsondenpotenzial in der Stadt Zürich, Schlussbericht, Amt für Hochbauten Stadt Zürich, 2014.
[28] S. Signorelli, Geoscientific Investigations for the Use of Shallow Low-Enthalpy Systems, Doctoral Thesis, ETH Zurich, 2004, https://doi.org/10.3929/ethz-a-004818477.
[29] E. Vitriu, G. Arnó Pons, I. Herms, J.J.d. Felipe Blanch, 3D modeling to evaluate the thermal interferences between borehole heat exchangers in a Mediterranean area, in: European Geothermal Congress 2019: the Hague, 11-14 June 2019: Proceedings, 2019, pp. 1–9.
[30] M.L. Fascì, A. Lazzarotto, J. Acuna, J. Claesson, Analysis of the thermal interference between ground source heat pump systems in dense neighborhoods, Sci. Technol. Built. Environ. 25 (2019) 1069–1080, https://doi.org/10.1080/23744731.2019.1648130.
[31] P. Bayer, M. de Paly, M. Beck, Strategic optimization of borehole heat exchanger field for seasonal geothermal heating and cooling, Appl. Energy 136 (2014) 445–453, https://doi.org/10.1016/j.apenergy.2014.09.029.
[32] G. Attard, P. Bayer, Y. Rossier, P. Blum, L. Eisenlohr, A novel concept for managing thermal interference between geothermal systems in cities, Renew. Energy 145 (2020) 914–924, https://doi.org/10.1016/j.renene.2019.06.095.
[33] K. Link, Statistik der geothermischen Nutzung in der Schweiz – Ausgabe 2018, EnergieSchweiz, 2019. Technical Report.
[34] SIA, Sondes Géothermiques (SIA384/6), Swiss Society of Engineers and Architects, 2010. Technical Report.
[35] P. Eskilson, Thermal Analysis of Heat Extraction Boreholes, Doctoral Thesis, University of Lund, Sweden, 1987.
[36] V.D. ASIT, Cadastre de géothermie basse température, URL, www.asitvd.ch/md/f8c427d3-dc9e-4864-c593-f763b122e824, 2019.
[37] SITG, Cadastre technique du sous-sol, URL, https://ge.ch/sitg/fiche/6435, 2019.
[38] S. Kavanaugh, K. Rafferty, Geothermal Heating and Cooling: Design of Ground-Source Heat Pump Systems, ASHRAE, 2014. Technical Report.
[39] J. Spitler, M. Bernier, Vertical borehole ground heat exchanger design methods, in: Advances in Ground-Source Heat Pump Systems, Elsevier, 2016, pp. 29–61, https://doi.org/10.1016/B978-0-08-100311-4.00002-9.
[40] S. Schneider, P. Hollmuller, P. Le Strat, J. Khoury, M. Patel, B. Lachal, Spatial–temporal analysis of the heat and electricity demand of the Swiss building stock, Front. Built. Environ. 3 (2017) 53, https://doi.org/10.3389/fbuil.2017.00053.
[41] GeoMol Team, GeoMol – Assessing Subsurface Potentials of the Alpine Foreland Basins for Sustainable Planning and Use of Natural Resources – Project Report, LfU, Augsburg, 2015. Technical Report.
[42] Swisstopo, swissTLM3D Version 1.6, Swisstopo, 2018. Nachführungsinfo 2018.
[43] V.D. ASIT, Cadastre - MO et NPCS - thème Biens-fonds, URL, www.asitvd.ch/md/03d4716b-66af-f4d4-99a2-83406987ad32, 2019.
[44] SITG, Parcelles de la mensuration, URL, https://ge.ch/sitg/fiche/8450, 2020.
[45] Groupe de travail PGG, Evaluation du potential géothermique du Canton de Genève (PGG), Rapport de synthèse, PGG, Genève, Switzerland, 2011.
[46] H. Li, X. Li, C.K. Soh, An integrated strategy for sustainable development of the urban underground: from strategic, economic and societal aspects, Tunn. Undergr. Space Technol. 55 (2016) 67–82, https://doi.org/10.1016/j.tust.2015.12.011.
[47] J. Claesson, S. Javed, An analytical method to calculate borehole fluid temperatures for time-scales from minutes to decades, Build. Eng. (2011) 11.
[48] J. Claesson, P. Eskilson, Conductive heat extraction to a deep borehole: thermal analyses and dimensioning rules, Energy 13 (1988) 509–527, https://doi.org/10.1016/0360-5442(88)90005-9.
[49] SIA, Klimadaten für Bauphysik, Energie- und Gebäudetechnik (SIA 2028), Swiss Society of Engineers and Architects, 2010. Technical Report.
[50] MeteoSwiss, Daily Mean, Minimum and Maximum Temperature, Documentation of MeteoSwiss Grid-Data Products, Federal Office of Meteorology and Climatology MeteoSwiss, 2017.